Precise branching ratio measurement for the superallowed β^{+} decay of ^{26}Si: Completion of a second mirror pair

M. Bencomo, J. C. Hardy, V. E. Iacob, H. I. Park, L. Chen, V. Horvat, N. Nica, B. T. Roeder, A. Saastamoinen, and I. S. Towner

Phys. Rev. C **100**, 015503 — Published 26 July 2019

DOI: 10.1103/PhysRevC.100.015503

Precise branching ratio measurement for the superallowed β^+ decay of ^{26}Si: Completion of a second mirror pair

M. Bencomo,* J.C. Hardy,† V.E. Iacob, H.I. Park, L. Chen, V. Horvat, N. Nica, B.T. Roeder, A. Saastamoinen, and I.S. Towner
Cyclotron Institute, Texas A&M University, College Station, Texas 77843-3366, USA
(Dated: May 7, 2019)

As part of a continuing effort to test the unitarity of the Cabbibo-Kobayashi-Maskawa matrix, we have measured the branching ratio for the superallowed $0^+ \to 0^+$ β^+-decay transition from ^{26}Si to be 0.7569(14), a result with 0.18% relative precision. With this result, the ft value for the transition is now established with comparable precision to the well-known superallowed transitions currently used in the determination of V_{ud}. It also completes a second pair of mirror superallowed transitions, $^{26}\mathrm{Si} \to {}^{26m}\mathrm{Al}$ and $^{26m}\mathrm{Al} \to {}^{26}\mathrm{Mg}$, the ratio of whose measured ft values provides a sensitive test of the method used to calculate the isospin-symmetry-breaking correction δ_C needed to determine V_{ud}. Like the previously measured ratio for the mass-38 mirror pair, the new result agrees well with the calculation based on Woods-Saxon radial wave functions, and strengthens the case for rejecting the calculation that uses Hartree-Fock radial functions.

I. INTRODUCTION

Superallowed $0^+ \to 0^+$ nuclear β decays offer a valuable window on the vector current of the weak interaction. A growing number of such precisely characterized decays have been used to verify conservation of the vector current (CVC) and to obtain V_{ud}, the up-down quark-mixing element of the Cabibbo-Kobayashi-Maskawa (CKM) matrix. The precision so far achieved for V_{ud} is sufficient to provide the most demanding available test of the unitarity of that matrix: the sum of squares of the three top-row elements. For some time this sum has been consistent with unitarity to within $\pm 0.06\%$ [1, 2] but a very recent re-evaluation of the inner radiative correction casts that agreement in doubt [3]. Since any statistically significant deviation from CKM unitarity would signal the need for new physics beyond the electroweak standard model, improvements in the value of V_{ud}, particularly any reduction of its uncertainty, are of considerable importance.

To be useful in affecting the result for V_{ud}, the measured ft value for a superallowed transition must be very precise (and, of course, accurate). In the most recent survey of world data [1], 14 transitions with relative uncertainties between $\pm 0.01\%$ and $\pm 0.3\%$ were incorporated into the full analysis and extraction of V_{ud}. We report here the first precise measurement of the superallowed β-branching ratio for the $0^+ \to 0^+$ decay of ^{26}Si. With our result, the ft value for this transition reaches a precision of $\pm 0.18\%$, thus elevating it to become the 15th member of the select group of contributing transitions.

Although the addition of one more transition, in itself, has a relatively minor impact on V_{ud}, the ^{26}Si transition has particular significance. Like the ^{38}Ca superallowed decay, which we added five years ago [4, 5], the $^{26}\mathrm{Si} \to {}^{26m}\mathrm{Al}$ decay is one of the few accessible superallowed transitions to have a mirror decay partner, in this case $^{26m}\mathrm{Al} \to {}^{26}\mathrm{Mg}$. It becomes only the second one to have been precisely measured. As we pointed out for the mass-38 result [4], a high-precision comparison of the ft values from a pair of mirror superallowed decays is very sensitive to the model used to calculate the isospin-symmetry-breaking correction, δ_C, used to convert measured ft values into the corrected $\mathcal{F}t$ values needed to verify CVC and extract a value for V_{ud}.

Because the experiments have become so precise, the current error bar quoted for V_{ud} is dominated by theoretical uncertainties. Consequently we have focused our attention on transitions that can complete mirror pairs, with the goal of reducing the uncertainty on the isospin-symmetry-breaking correction by shrinking the number of acceptable model calculations to only those that agree with the precisely measured ft-value ratios. This can serve to reduce the V_{ud} uncertainty by up to 10% if none of the other correction terms were improved. The effect could have even greater impact if other corrections were improved as well.

Our measurement consisted of repetitive cycles, in which we deposited pure samples of accelerator-produced ^{26}Si, moved them rapidly to a shielded counting location, and recorded β-γ coincidences from their decay. By measuring the absolute intensity of the γ-ray peaks in the coincidence spectrum and comparing them to the total number of detected β particles, we determined the branching ratios for the β transitions that populated the γ-emitting states in ^{26}Al.

II. EXPERIMENT

A. Production

We produced ^{26}Si ($t_{1/2}$= 2.245 s) using a 30A-MeV ^{27}Al beam from the Texas A&M University K500 super-

* mbencomo@comp.tamu.edu
† hardy@comp.tamu.edu

conducting cyclotron to initiate the $p\,(^{27}\mathrm{Al},\,2n)^{26}\mathrm{Si}$ reaction. The target was hydrogen gas, cooled by liquid nitrogen and held at 2.0 atm pressure in a cell located in the target chamber of the Momentum Achromat Recoil Spectrometer (MARS) [6]. The fully stripped ejectiles were analyzed by MARS according to their mass-to-charge ratio. Initially, working with a low-current primary beam, we inserted at the focal plane of MARS a 5 cm×5 cm position-sensitive silicon detector (PSSD) consisting of 16 strips, 1-mm thick. The PSSD was employed first for the identification of secondary reaction products, then to adjust the position and focus of the desired species.

Figure 1 shows the results obtained after the spectrometer had been tuned for ^{26}Si and the focal-plane acceptance slits set 1.2 cm apart (indicated by dashed lines in the figure). The projection to the right in the figure shows the total intensities of the different isotopes present in the extracted beam. That beam was 98.7% pure ^{26}Si, with the principal surviving impurities being ^{22}Mg, ^{23}Mg, ^{24}Al and ^{25}Al.

After the tuning and selection procedure was complete, the PSSD was removed from the beam path and the intensity of the primary beam increased. The nearly pure ^{26}Si beam passed out of the vacuum system through a 50-μm-thick kapton window; then through a 0.3-mm-thick BC-404 plastic scintillator, where the ions were detected; next through a set of aluminum degraders; and finally it was implanted in the 76-μm-thick aluminized Mylar tape of a fast tape-transport system. Since the impurities in the beam have different stopping powers in aluminum than does ^{26}Si, the degraders could be selected to nearly eliminate any impurities being stopped in the tape (See Sec. II C). As a consequence, the sample collected in the tape was >99.99% pure ^{26}Si.

During our measurement, the beam composition was checked daily by our reinserting the PSSD at the focal plane in MARS and recording the spectrum of deposited energy as a function of position. No significant changes were observed throughout the experiment.

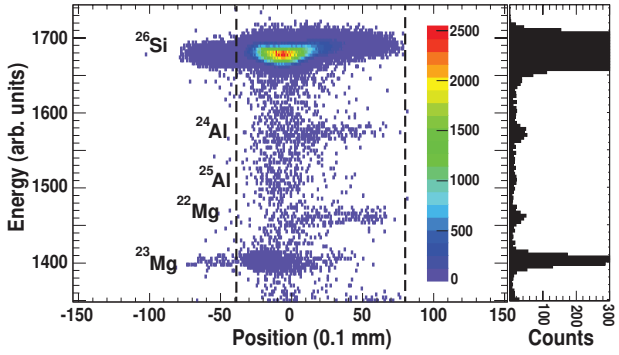

FIG. 1. (Color on-line) The main figure shows the deposited energy versus position as obtained with the PSSD in the MARS focal plane with the acceptance slits set asymmetrically, 1.2 cm apart as indicated by the dashed lines. Lighter mass impurities, not shown in the figure, are weaker and have substantially longer ranges; so they were not stopped in the tape and play no role in the measurement. The projection on the right illustrates the intensity of extracted beams. To set the scale, note that the the intensity of the ^{23}Mg impurity was 0.75% that of ^{26}Si.

B. Data Collection

To study the ^{26}Si decay, we collected data in repetitive cycles. Each cycle began with ^{26}Si being collected in the tape for 5 s, during which time the rate of accumulation was recorded by the plastic scintillator located just after the exit of the MARS vacuum system. After collection was complete, the beam was interrupted and the tape moved in 230 ms to deliver the collected sample to a well-shielded counting location, about 90 cm away, where time-tagged β-γ coincidence events were recorded for another 5 s, after which the beam was restored and the cycle repeated. During this experiment more than 25,000 cycles were recorded from 57 individual runs, averaging 447 cycles per run.

At the counting location, a 1-mm-thick BC-404 plastic scintillator for the detection of β particles was located 3 mm from one side of the tape-implanted source. On the opposite side, facing it at a distance of 151 mm from the tape, was a high-purity germanium (HPGe) detector for γ rays. The distance between the stopped tape and the HPGe detector was measured and recorded during every cycle with a laser triangulation device that allowed us to determine the distance with an accuracy of ± 30 μm [7]. Since the HPGe detector efficiency has been calibrated precisely at a source-to-detector distance of 151.0 mm, the measured distance was used to adjust the detector efficiency calibration during analysis. Over the course of the experiment, the measured distance averaged 151.2 mm, so the necessary adjustment was very small.

During the measurement, our data-acquisition system generated a "master trigger" by identifying the arrival of a β particle and a γ ray within 2 μs of one another. This signaled the occurrence of a potentially coincident β-γ event and initiated acquisition. For each such event, we recorded both the β and the γ-ray energies, the precise time-difference between their arrivals, and the time when the event itself occurred relative to the beginning of the counting period. In addition to individual event recording, we also stored the following parameters for each cycle: the rate of accumulation of ^{26}Si ions in the tape as a function of time during the collection period; the laser distance reading; and the total number of β and γ-ray singles recorded during the counting period. The same discriminator signals used in creating the master triggers were used to scale the β and γ-ray singles. Finally, throughout the measurement, the electronic dead times for the coincidence channel and the two singles channels were measured continuously with signals from a constant-frequency pulse generator being recorded in coincidence with the gating signals from each channel.

The room background was measured during the ex-

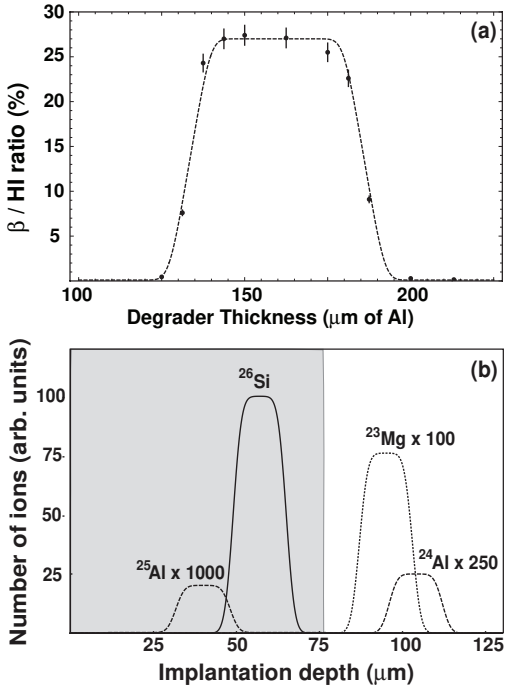

FIG. 2. (a) Degrader scan showing the β/HI ratio as a function of Al thickness. The black circles with uncertainties are the measured data; the line is a fit based on the implantation profile, as described in the text. (b) Derived implantation profiles for ^{26}Si and the nearby impurities, with the final degrader setting of 146 μm. Beams enter from the left and the gray region corresponds to the actual thickness of the Mylar collection tape. Only the ions within this region are collected in the sample. The ^{22}Mg ions are off-scale to the right.

periment in order to determine its contribution to the β-γ coincidence data and the β-singles rate. We did this by disabling the transport-tape motion but otherwise leaving the beam-cycling and data-acquisition process unchanged. These cycles differed from normal measurement cycles only in that the collected sample never reached the counting location. Under these conditions, β-γ coincidences were negligibly few, and the β-singles rate dropped to 0.6 β/s, about 4 orders of magnitude less than the β count rate during a normal cycle. Nevertheless, this measured background rate for β singles was incorporated into our analysis.

C. Elimination of impurities

For a precision measurement of the type reported here, it is essential to eliminate, or at least minimize, impurities in the collected samples. Already we have demonstrated that the beam exiting MARS was nearly pure, but we found we could entirely remove the remaining impurities by carefully adjusting the thickness of the aluminum degraders that the beam passed through before entering the collection tape.

Our degrader assembly consisted of two wheels around which a sequence of different thickness aluminum foils had been mounted. We could rotate the wheels remotely using stepping motors controlled by Arduino microcontrollers [8]. After MARS had been tuned, but before our measurement began, we recorded the number of β particles detected at the counting location as a function of degrader thickness. The result is shown as the data points in Fig. 2(a). So as to be independent of random changes in the primary beam current, we normalized the number of observed β events in each cycle by the number of heavy ions (HI) detected in the plastic scintillator located at the exit of MARS, upstream from the degraders. This is the β/HI ratio plotted on the vertical scale. Evidently, with only 125 μm of aluminum, the ^{26}Si ions punch through the tape while, at the other end of the scale, 195 μm of aluminum is sufficient to stop all ^{26}Si ions before they reach the tape.

Next, using the SRIM [9] code we calculated the range and distribution of ^{26}Si ions passing through the plastic scintillator, aluminum degraders and Mylar collection tape. By also incorporating the momentum spread set by slits in MARS ($\Delta p/p = 0.69\%$), we arrived at a rectangular range profile, with which we convolved a Gaussian function to obtain realistic tailing. After only a few minor adjustments, the resulting profile can be seen in Fig. 2(a) to agree well with the results of the measured degrader scan. With the ^{26}Si profile confirmed, we used the same shape for the impurities, with their range relative to that of ^{26}Si being determined from a SRIM calculation.

Finally, armed with this information, we chose a thickness of aluminum degrader, 146 μm, which ensured that all ^{26}Si ions were implanted in the tape while all the impurity ions except ^{25}Al punched through. As seen in Fig. 2(b), the range separation is clean. The intensity of the remaining impurity, ^{25}Al, is 0.017% that of ^{26}Si and its half-life is three times longer, so its contribution to the collected sample's β activity must be less than 0.01%. We consider this to be negligible.

III. ANALYSIS

The β decay of ^{26}Si offers a superallowed branch, which directly feeds the 0^+ 228-keV isomeric state of its daughter ^{26}Al, but there are also competing Gamow-Teller branches to higher excited 1^+ states. Each of the 1^+ states emits a prompt γ ray to the isomeric state. A simplified decay scheme appears in Fig. 3. With the isomeric state emitting no prompt γ ray, the superallowed-transition's branching ratio cannot be determined directly from the γ-ray spectrum. Instead we use that spectrum to determine the total percentage branching to all 1^+ states, and subtract the result from 100%. In practice, we actually determine the absolute branching ratio to the 1058-keV state, the one most strongly populated; then obtain the total Gamow-Teller branching using the relative intensities of the other γ-ray peaks.

The fact that the observed Gamow-Teller transitions

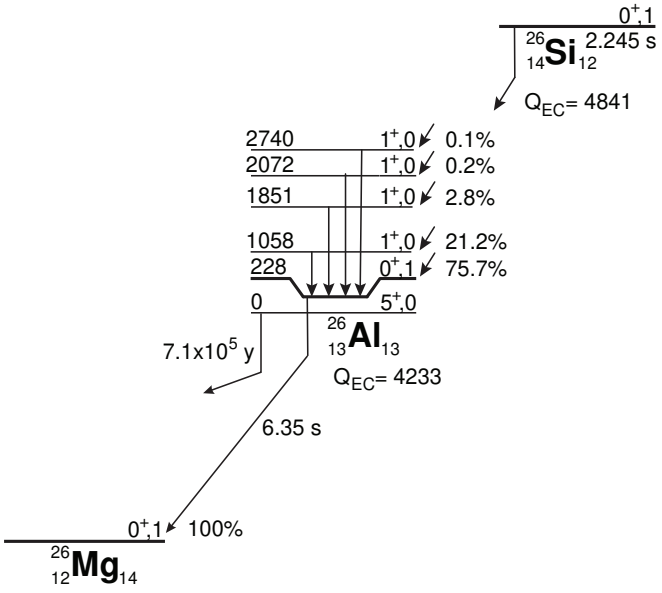

FIG. 3. Decay scheme of ^{26}Si showing the five strongest β branches and the most intense subsequent γ-ray transitions in ^{26}Al. The level information is from Ref. [10]; the β branching ratios are from this work. All energies are in keV. The Q_{EC} values refer to the superallowed transitions.

from ^{26}Si sum to a relatively small value, ∼24%, works to our advantage in achieving high precision for the superallowed branching ratio. The relative precision achieved in the measurement of the total Gamow-Teller strength is improved by a factor of three when that measured value is subtracted from 100% and the same uncertainty is applied to the ∼76% superallowed branch.

We determine the branching ratio to the 1058-keV 1^+ state in ^{26}Al from the ratio of the number of β-coincident 829-keV γ rays observed relative to the total number of positrons emitted from ^{26}Si. In general, if a particular state i is populated by β decay and de-excites by emitting a γ ray, γ_i, then the branching ratio R_i for the β transition feeding the state is given by

$$R_i = \frac{N_{\beta\gamma_i}}{N_\beta}\frac{\epsilon_\beta}{\epsilon_{\gamma_i}}\frac{}{\epsilon_{\beta_i}}, \qquad (1)$$

where $N_{\beta\gamma_i}$ is the number of β-γ coincident counts observed in the γ_i peak, N_β is the number of recorded β particles, ϵ_{γ_i} is the efficiency of the HPGe detector for detecting γ_i rays, ϵ_{β_i} is the efficiency of the plastic scintillator for detecting the β's that populate state i, and ϵ_β is the average efficiency for detecting β's from all ^{26}Si transitions.

It is important to recognize that this equation strictly applies only to the simplest case. It assumes that state i is neither fed by another γ transition, nor emits any γ ray other than γ_i; and, in our application to positron decay, the equation ignores the small contribution from electron-capture decay[1]. As it happens, in the case of ^{26}Si decay to the 1058-keV state, only very small deviations from simplicity occur; they will be handled in Sec. IV. Before that, we shall describe the initial processing of the data, and detail how the terms on the right side of Eq. (1) are determined for the β transition to the 1058-keV state.

A. Cycle selection

Out of the ∼25,000 data cycles recorded during the experiment only those that met certain criteria were retained. The first filtering criterion was applied to the number of implanted ^{26}Si ions detected by the BC-404 scintillator at the exit of MARS. Only cycles with a collection rate between 2,000 and 34,000 ions/s were accepted, thus eliminating cycles with very little or no beam, and those with abnormally high beam currents.

The second criterion was based on the ratio of the number of beta particles detected to the number of ^{26}Si ions implanted for each cycle, with limits set to accept those cycles having between 85-100% of the maximum value for each run. This rejected cycles in which the tape transport system did not move the sample to the central position between the β and γ-ray detectors. If the sample is located too far from the center it affects $\epsilon_{\gamma i}$ (though not $\epsilon_\beta/\epsilon_{\beta i}$).

With the third and final filter, we rejected cycles for which the distance between the HPGe detector and the tape deviated by more than ±0.3 mm from the mean value of 151.2 mm, as determined from the laser-sensor reading stored for each cycle. This allowed us to take full advantage of the precise calibration of the detector.

After the selection was complete, 23,430 cycles (92% of the original) remained. This was the data set used for all subsequent analysis. Note, though, that for the first part of the analysis we subdivided these data into three groups of cycles, depending upon their recorded counting rates. Since some corrections, such as for dead-time, depend sensitively on counting rate, we found it efficacious to apply these corrections to each group separately, only combining the three groups later to test for consistency and then apply the rate-independent corrections. For statistical reasons, the three groups were chosen to have similar coincident-event totals.

B. Eliminating random coincidences

There is a finite probability that two separate events from independent decays could occur closely spaced in

[1] Eq. (1) also ignores any possible contribution from internal conversion, but that is negligibly small for the relatively high-energy γ-ray transitions in this low-Z nucleus.

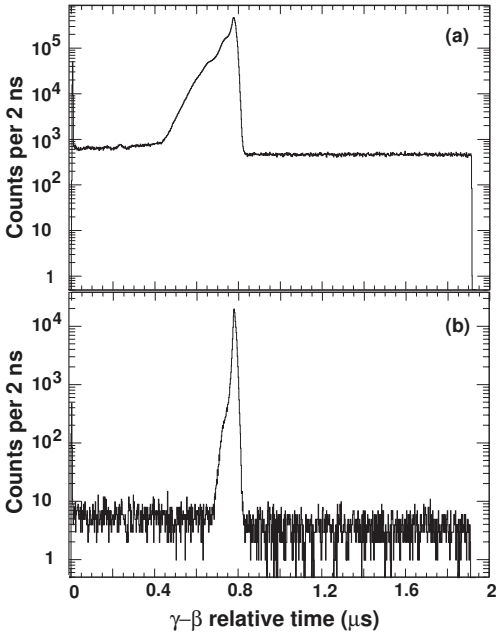

FIG. 4. (a) Spectrum of measured time intervals between the arrival of a γ ray and the electronically delayed signal from the β detector, for all identified coincidence events. (b) Measured time-interval spectrum for events corresponding only to the 829-keV γ ray.

time and be mistaken for a coincidence. The effects of such random coincidences can be eliminated with the help of the spectrum of time-differences between the detection of a γ ray and the subsequent arrival of an electronically delayed signal from the positron detector, as measured with a time-to-digital converter (TDC).

The time spectrum for all events is shown in Fig. 4(a). The "prompt" peak corresponds to true coincident events, while the flat distribution is due to random coincidences. The prompt peak has a noticeable tail to the left, which occurs because a wide range of γ-ray energies is involved. Lower energy γ rays trigger the TDC later than high energy ones, which results in shorter times before the arrival of the signal from the corresponding β particle. The single-channel peak at zero time is an artifact resulting from the way in which we establish the master trigger. It contains only random coincidences, and its height is proportional to the time-width of the β-derived timing signal used to establish the existence of a coincidence. Figure 4(b) shows the time spectrum corresponding to the single γ-ray peak at 829 keV. As expected, this prompt peak is much narrower.

With the time spectrum in Fig. 4(a) we could produce a γ-ray spectrum from which all random coincidence events have been removed. First, we gated on the part of the time spectrum containing the prompt peak, and then on the flat parts on either side containing random coincidences. The γ-ray spectrum obtained from the flat regions was normalized to the same time width as the prompt-peak gate; then it was subtracted from the spectrum gated on the prompt peak. The resulting spectrum, shown in Fig. 5, is free of random-coincidence events: all γ-ray peaks belong to the decay of ^{26}Si.

This spectrum exhibits a prominent 511-keV peak due to positron annihilation; the four γ rays of interest, which de-excite the 1^+ states in ^{26}Al; and two true-coincidence sum peaks. Of the latter, the "511 + 171" peak corresponds to the sum of two annihilation photons, one of which has backscattered from the plastic scintillator into the HPGe detector; while the "511 + 829" peak results from coincident summing of annihilation radiation from the positron that populates the 1058-keV state with the 829-keV γ ray that de-excites the state.

C. Efficiency calibrations

It is clear from Eq. (1) that in order to determine the superallowed branching ratio we need to rely on the precise absolute efficiency calibration of the HPGe detector and a reasonable understanding of the energy dependence of the β-detector efficiency.

The absolute efficiency, ϵ_γ, of our HPGe detector at a source-to-detector distance of 151 mm was meticulously calibrated 15 years ago [11] with 13 individual sources from 10 different radionuclides – ^{48}Cr, ^{60}Co, ^{88}Y, ^{108m}Ag, ^{109}Cd, ^{120m}Sb, ^{133}Ba, ^{134}Cs, ^{137}Cs and ^{180m}Hf – anchored by two ^{60}Co sources specially prepared by the Physikalisch-Technische Bundesanstalt (PTB), with activities certified to $\pm 0.06\%$ [12]. At the same time, we made measurements specifically designed to determine the physical dimensions and location of the Ge crystal in its housing. This information was then used as input to Monte Carlo calculations performed with the electron and photon transport code CYLTRAN [13]. The relative and absolute efficiency measurements combined with Monte Carlo calculations provide us with an uncertainty of $\pm 0.2\%$ in the efficiency curve between 50 and 1400 keV [11]. A little later, sources of ^{24}Na, ^{56}Co and ^{66}Ga were

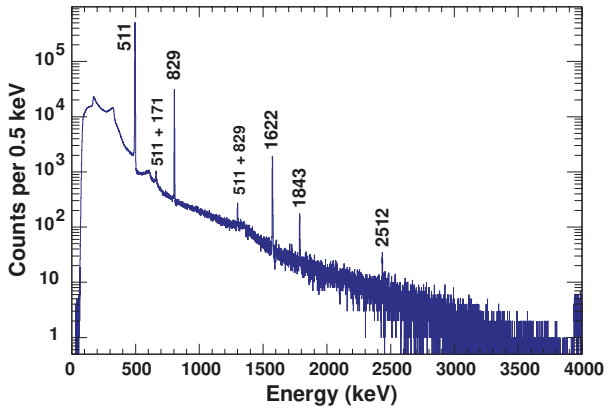

FIG. 5. Spectrum of β-delayed γ rays observed in coincidence with positrons from the decay of ^{26}Si. All peaks are identified with their energies in keV.

used to extend the region of calibration up to 3500 keV with an uncertainty of ±0.4% in the extended energy region [14]. Since then, the HPGe detector has been, and continues to be, kept at liquid nitrogen temperature at all times to preserve its calibration. It is also checked periodically with the PTB calibration source to ensure that no change in efficiency has occurred.

As already noted, the average source-to-detector distance during our ^{26}Si decay measurement was 151.2 mm, 0.2 mm greater than the distance used for calibration. We accounted for this small difference using the CYLTRAN Monte Carlo code, with which we calculated the efficiencies for the four main γ rays of interest. They are listed in the third column of Table I.

Our β detector is a 1-mm-thick Bicron BC404 scintillator disc recessed into a cylindrical Lucite light guide, which is optically coupled in turn to a photomultiplier tube. Its response function has been extensively characterized as a function of β-particle energy by a combination of GEANT4 [15] Monte Carlo simulations and measurements with ^{133}Ba, ^{137}Cs and ^{207}Bi sources, all three of which emit conversion electrons, and one, ^{137}Cs, emits β-decay electrons. The agreement between measurements and simulations was found to be excellent [16]. Since those studies were completed ten years ago, we have had similar success comparing our calculations to positron emitters: the standard source ^{22}Na, and the accelerator-produced superallowed emitter ^{38}Ca [5]. We have also demonstrated that the EGSnrc Monte Carlo code [17] produces equally good agreement with measurements and runs more rapidly than GEANT4, so we have used the former code in the present analysis.

The absolute efficiency of the β detector is not required for our measurement, but its dependence on energy is. If the detector response function were completely independent of energy, the term $\epsilon_\beta/\epsilon_{\beta i}$ in Eq. (1) would be equal to unity. However, the efficiency does change slightly as a function of the end-point energy $E_{\beta max}$ because the fixed low-energy electronic threshold removes a slightly different fraction of the β energy spectrum for different end-point energies. This effect is important because any change in β efficiency from one transition to another affects the measured intensities of the coincident γ rays.

TABLE I. HPGe detector efficiencies for the γ rays that deexcite the states at energy E_{xi}; and scintillator efficiency ratios for the βs that populate those states. Also shown are the ratios of electron-capture to positron emission for the β transitions.

E_{x_i} [a] (keV)	E_{γ_i} (keV)	ϵ_{γ_i} (%)	$E_{\beta max}$ (keV)	$\epsilon_\beta/\epsilon_{\beta_i}$	ec/β^+
228.3	–	–	3818.8	0.9985	0.000636
1057.7	829.4	0.2763(6)	2989.4	1.0029	0.001320
1850.6	1622.3	0.1729(7)	2196.5	1.0162	0.003327
2071.6	1843.3	0.1569(6)	1975.5	1.0267	0.004567
2740.0	2511.7	0.1214(5)	1307.1	1.0819	0.016283

[a] Values taken from Ref. [10].

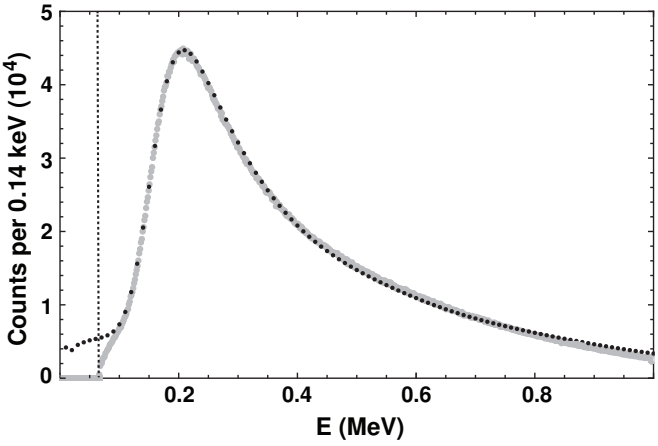

FIG. 6. The measured energy deposition (gray) in the β detector for the decay of ^{26}Si compared to the simulated spectrum (black dots) obtained from EGSnrc. The vertical dotted line at 60 keV marks our threshold.

The energy deposition we recorded in the β detector during the ^{26}Si-decay measurement is compared with EGSnrc-generated Monte Carlo calculations in Fig. 6. In the fifth column of Table I we list the efficiency ratio $\epsilon_\beta/\epsilon_{\beta i}$ for each individual β transition, which have all been calculated with the same code and the same 60-keV threshold. Excellent spectral agreement in the figure lends credence to the ratios listed in the table, which appear without uncertainties because all are quite near unity and have uncertainties that are negligible in the present context. Although not required for the analysis, the total efficiency ϵ_β is calculated to be ∼46%.

D. β singles

The number of β-singles counts we record in our experiment includes not only the β particles emitted by ^{26}Si but also those emitted by its daughter ^{26m}Al, as well as small contributions from room background and decay γ rays registering in the β scintillator. Since the term N_β in Eq. (1) refers only to β particles from the decay of ^{26}Si, the other contributions must be quantified and subtracted from the recorded β singles to yield N_β.

1. *Parent-daughter β fraction*

We deal first with the contribution from β decay of the daughter nucleus ^{26m}Al. Although no ^{26m}Al was deposited in the tape directly, it naturally accumulated as a daughter product of ^{26}Si during the collection period, and was delivered with the collected sample to the counting location, where it continued to accumulate during the counting period. It, too, β decays but with a longer half-life of 6.34602(54) s, compared with 2.2453(7) s for ^{26}Si

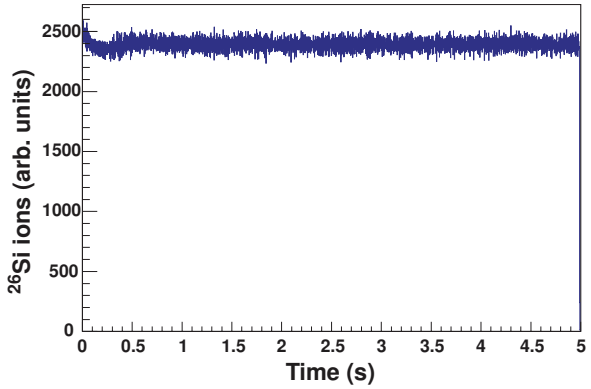

FIG. 7. Cumulative time profile of deposited ^{26}Si as recorded for all selected cycles. The initial drop in intensity is caused by the decrease in local density of the hydrogen in the target cell as the primary beam heats the gas around its path. A fan located inside the gas target mitigates the effect and ensures a rapid transition to stable conditions.

[1]. Thus, by the time the counting period began a substantial fraction of the deposited ^{26}Si had converted to ^{26m}Al; however, this loss was partially offset by the fact that during the 5-s counting period a considerably larger proportion of β particles were emitted from ^{26}Si than from the longer lived ^{26m}Al.

Because the collection and counting periods were precisely measured, and the half-lives of ^{26}Si and ^{26m}Al are well known, the ratio of total decays accumulated from the two activities during the counting period can easily be calculated provided that the ^{26}Si implantation rate is known as a function of time during the collection period. This information is provided by Fig. 7, which shows a cumulative time profile of the implanted beam as recorded from the scintillator located at the exit of MARS.

The last piece of information required to obtain the parent-daughter fraction is our β detector's relative efficiency for the two activities. Just as we have seen in Sec. III C that the β-detector efficiency is different for different energy transitions from ^{26}Si, so it differs between the decays of ^{26}Si and ^{26m}Al, which have different Q_{EC} values and different mixes of individual β transitions. Based on the same EGSnrc calculations, we determine that our efficiency for detecting the β particles from ^{26m}Al is 0.25% less than it is for β particles from ^{26}Si.

Combining parent-daughter decay probabilities with the small difference in detector efficiencies, we obtain 0.5688(4) as the fraction of detected β particles that can be attributed to ^{26}Si.

2. γ rays registering in the β detector

There is a very small probability that γ rays produced in the decay of ^{26}Si get counted in the 1-mm-thick β scintillator. This is irrelevant for annihilation radiation, which can be thought of as equivalent to a β particle in contributing to a valid coincidence trigger; but it is very relevant for all other γ rays provided that they are detected without the corresponding β particle that feeds the transition being detected. Given the insensitivity of a thin plastic scintillator to γ rays, the high (46%) β-detection efficiency and the fact that only 24% of ^{26}Si decay strength leads to γ-ray emission, this effect is very small. Using EGSnrc Monte Carlo calculations, we determine it to account for 0.117(5)% of the total counts recorded in the β detector.

3. Results for N_β

The input data used to derive N_β is presented in Table II. From the total number of β-detector counts, we first remove the background, then correct for the single γ-rays counted in the β detector. Finally we apply the calculated fractional contribution of ^{26}Si to the remaining number of β singles. The final result for N_β appears in the last line of the table.

E. β-coincident γ-rays

The primary experimental source for $N_{\beta\gamma 829}$, the number of β-coincident 829-keV γ rays, is the integrated area of the 829-keV γ-ray peak gated by the prompt peak in the γ-β time spectrum; see Sec. III B and Fig. 4(b) for details. Our procedure for extracting the peak area – and areas of other peaks in the spectrum – was to use a modified version of GF3, a least-squares peak-fitting program in the RADWARE package [18]. A skewed Gaussian peak with a smoothed step function, and linear background in the peak region were sufficient to properly describe the data in the spectrum. This replicates the method we used in the original calibration of the HPGe detector.

This is not the full story though. There are several small corrections that must be applied to the peak area before it can be used as input to Eq. (1). In the following sections, we describe and evaluate corrections to account for coincidence summing, dead-time losses, pileup and other small effects.

TABLE II. Derivation of N_β from the total number of single events recorded in the β detector.

Quantity	Value	Source
Total β-detector counts	$5.27226(23)\times10^8$	
Background	$-6.982(25)\times10^4$	Section II B
Detected γ rays	$\times0.99883(5)$	Section III D 2
^{26}Si fraction of β's	$\times0.5688(4)$	Section III D 1
N_β (^{26}Si)	$2.99496(211)\times10^8$	

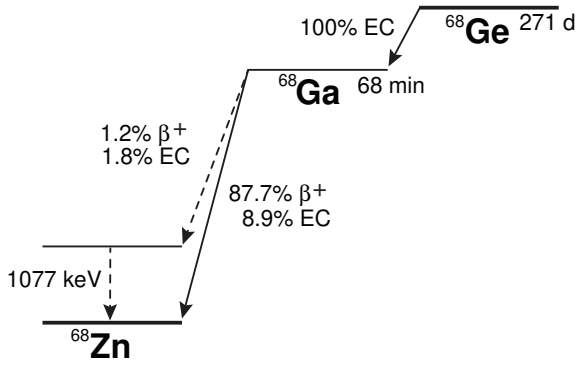

FIG. 8. Dominant decay branches in the decay of ^{68}Ge, taken from Ref. [19].

1. Real coincidence summing

Because each 829-keV γ ray from the decay of the 1058-keV state in ^{26}Al is accompanied by a positron from the ^{26}Si β^+-decay branch that populated the state, there is a significant probability that the 829-keV γ ray and the 511-keV radiation from positron annihilation will reach the HPGe detector simultaneously and be recorded as a single γ-ray event with a combined energy of 1340 keV; a peak at this energy is indeed apparent in Fig. 5. Such summing steals counts from the 829-keV peak of interest, and must be corrected for. However, the loss is greater than just the counts in the 1340-keV peak: It comes not only from the summing of the two full-energy peaks, but also from summing of full-energy 829-keV events with 511-keV photons that Compton scatter in the HPGe crystal, depositing less than their full energy. The latter events are not identifiable in the spectrum since they are indistinguishable from the continuum. To account for all such losses, we need to know the full response function of our detector for 511-keV photons. In particular, we require the ratio of the detector's total efficiency to its full-energy-peak efficiency – the total-to-peak ratio – for 511-keV photons.

We determined the total-to-peak ratio in an off-line decay measurement using a commercially available source, ^{68}Ge, with the same geometry and nearby surroundings as pertained to the on-line experiment. As shown in Fig. 8, ^{68}Ge decays by electron capture to ^{68}Ga, which in turn decays to ^{68}Zn, mostly by positron emission. Thus, its γ-ray spectrum is dominated by annihilation radiation and provides a direct measure of the detector response function above the 90-keV threshold energy set by the electronics. With the short extrapolation to zero energy provided by Monte Carlo calculations, we determined the total-to-peak ratio to be 3.59(3). This result multiplied by the area of the 1340-keV sum peak, which contains 1435(63) counts, determined 5152(230) to be the total loss from the 829-keV peak due to coincidence summing with annihilation radiation. Compared with the total number of counts observed in the 829-keV peak, this represents a +3.1(1)% correction.

Just as summing with annihilation radiation leads to lost 829-keV peak counts, so does real-coincidence summing of 829-keV γ rays with external bremsstrahlung emitted from the deceleration of positrons in or near the β detector. In this case, though, there is no sum peak to signal its presence; instead we have only a continuous energy spectrum, which is indistinguishable from the summed Compton distributions from all detected γ rays. To determine the contribution of bremsstrahlung to the γ-ray spectrum, we took the areas of all γ-ray peaks including the 511-keV one, and multiplied each by its corresponding total-to-peak ratio[1]. The sum of products was then subtracted from the total number of counts in the γ-ray spectrum, with the difference being attributed to the contribution from bremsstrahlung. From this result and the known full-energy-peak efficiency of the detector for 829-keV γ rays, we calculated the probability for summing. The resulting loss from the 829-keV peak was determined to be 0.2(1)% of the total.

2. Dead time and pileup

During our experiment, as described in Sec. II B we continuously monitored system dead times for β-singles, γ-singles, and β-γ coincidence events. From Eq. (1) it is evident that dead time in the β-detection system must affect both numerator and denominator equally. Because of this, and the fact that the 450-ns dead time per β event is very small, we can neglect its effect on our result. In contrast, the HPGe detector signals are much slower and are affected by both dead time and pile-up. The size of the corrections required to compensate for these effects depends on the rates both of coincident γ rays and of γ-ray singles.

Both dead time and pile-up remove legitimate events from the γ-ray peak of interest so we treat them together. We determined the pile-up time for γ rays to be 17 μs based on their signal pulse shape. Since γ-ray singles events are not encoded, their dead time is much shorter than this pile-up time, so it is the latter which determines the losses for these events. However, the dead time per event for coincident γ rays, which are encoded, was measured online to be 25.6 μs, a value that is larger than, and hence subsumes, the pile-up time. We calculated the total loss from both types of γ-ray event by integrating the dead-time losses over the whole counting period, taking into account the decrease in rate from the decay of ^{26}Si as well as the growth and decay of its daughter. As discussed in Section III A, the data were divided into

[1] Total-to-peak ratios for the non-annihilation γ rays were determined from a combination of experiment and Monte Carlo calculations. Except that it was applied to our specific experimental conditions, the method was the same as that described in Ref. [11].

three evenly split groups, depending on their β-singles rate, and each group was analyzed separately. Losses for the low-rate group were found to be 0.54(7)%, rising to 1.08(14)% and 1.54(18)% for the medium- and high-rate groups.

3. Preemption of real coincidences

There is a small probability that a real coincidence gets lost if it is preempted by a random coincidence. This can occur if a master trigger is generated by a real β-γ coincidence, which starts our timing clock (the analog-to-digital converter), but a random β event stops the clock before the true coincident β does. The magnitude of this effect can easily be calculated from the known rate of β signals and the time between the clock start and the appearance of the prompt peak; see Fig. 4. Like dead time, preemption of real coincidences is rate dependent. We calculate the losses to be 0.13(1)%, 0.34(3)% and 0.48% for the three data groups, from low to high rates.

4. Results for $N_{\beta\gamma}$

The corrections just described fall into two categories: those that are rate dependent (dead time, pile-up and random preemption) and those that are not (real-coincidence summing with annihilation radiation and bremsstrahlung). Table III shows the process we followed in implementing the various corrections to obtain the value of $N_{\beta\gamma 829}$ from the measured area of the 829-keV peak. The top portion of the table presents the rate-dependent corrections applied to the medium-rate data group as an illustration. Then the bottom portion of the table applies the remaining rate-independent corrections to the full data set. The final value of $N_{\beta\gamma 829}$ appears in the last row.

TABLE III. Derivation of $N_{\beta\gamma 829}$ from the total number of events in the 829-keV peak in the β-coincident γ-ray spectrum. The rate-dependent corrections are given only for the mid-rate group while other corrections are applied to the full data set.

Quantity	Value	Source
Medium-rate data:		
Area of 829-keV peak	63,223(279)	
Dead time/pileup	×1.0108(14)	Section III E 2
Random preemption	×1.0034(3)	Section III E 3
Corrected area	64,120(298)	
Full data set:		
Corrected 829-keV peak area	169,168(750)	
511-keV summing	×1.031(1)	Section III E 1
Bremsstrahlung summing	×1.0020(10)	Section III E 1
$N_{\beta\gamma 829}$	174,756(793)	

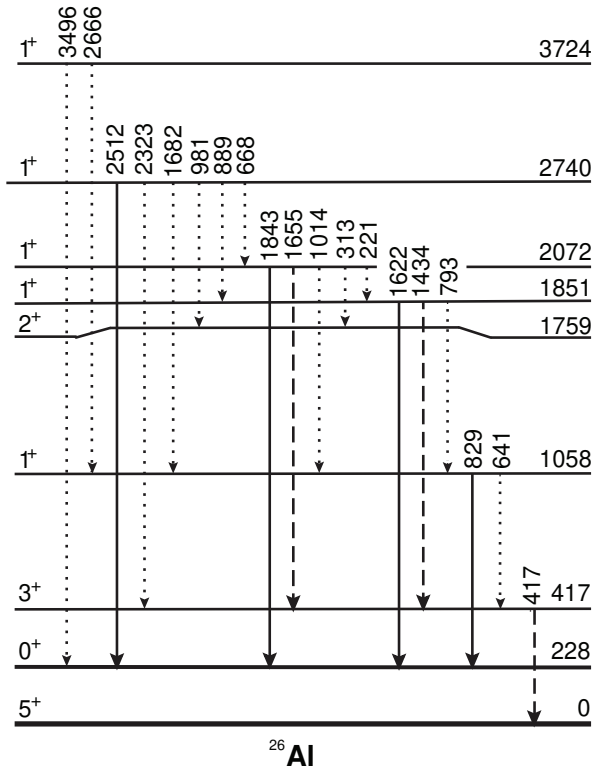

FIG. 9. Partial level scheme of ^{26}Al, showing the excited states populated by the β decay of ^{26}Si and the γ transitions that occur or may occur following the β decay [10]. The transitions of principal interest (also shown in Fig. 3) are represented by solid lines. The dashed lines indicate weaker observed transitions while dotted lines identify even weaker possible transitions that are not observed and for which we can only set an upper limit.

This completes the data input required to evaluate Eq. (1). However, as noted in Sec. III, that equation applies to an ideal case in which the daughter state is fed only by β decay, and decays only by a single electromagnetic transition. To extract the precise β-branching ratio, we must take account of other weak γ transitions that are observed, and set limits on those that are not. These weaker transitions are discussed in the next section.

F. Relative γ-ray intensities

Up to this point, we have only mentioned the four predominant γ-ray transitions to the ^{26}Al ground state that follow β-decay branches from ^{26}Si. Other electromagnetic transitions within ^{26}Al can occur and, if of significant strength, they would impact derivation of the β branching ratios. Our search for such weak γ rays was guided by the known level scheme of ^{26}Al and by previous studies [20–24]. Figure 9 illustrates the transitions we investigated in the β-coincident γ-ray spectrum of Fig. 5. All peak areas were determined by the same

TABLE IV. Intensities of β-delayed γ rays from the β^+ decay of ^{26}Si, expressed relative to the 829-keV transition.

E_γ	I_γ						
(keV)	Ref. [20]	Ref. [21]	Ref. [22]	Ref. [23]	Ref. [24]	This work	Adopted
221.0					0.000005(1)	<0.0015	0.000005(1)
312.6						<0.0017	<0.0017
416.9						0.0027(8)	0.0027(8)
640.9						<0.0007	<0.0007
668.4						<0.0008	<0.0008
792.9			<0.0027			<0.0005	<0.0005
829.4	1	1	1	1	1	1	1
889.4			<0.002			<0.0006	<0.0006
981.0			<0.0016			<0.0005	<0.0005
1013.9						<0.0005	<0.0005
1433.8			<0.00096		0.0009(1)	0.0015(6)	0.0009(1)
1622.3	0.149(16)	0.134(5)	0.1245(23)	0.1301(62)		0.1322(16)	0.1301(19)
1654.8			0.00145(32)		0.0014(1)	0.0017(7)	0.0014(1)
1682.3			<0.00058			<0.0004	<0.0004
1843.3	0.013(3)	0.016(3)	0.01179(27)			0.0130(7)	0.0120(3)
2323.2			<0.00028		0.000023(6)	<0.0002	0.000023(6)
2511.7			0.00282(10)			0.0032(5)	0.0028(1)
2666.1			<0.00015			<0.0012	<0.00015
3495.5			<0.00005			<0.0009	<0.00005

method we used for the 829-keV peak, as explained in Sec. III E. Because the data in our spectrum have been selected by a β coincidence, the relative peak intensities derived from the spectrum not only have to be adjusted for γ-ray efficiencies but also for the corresponding relative β-detector efficiencies and for the contribution of electron capture to the decay branch from ^{26}Si. The efficiencies and electron-capture fractions for the largest peaks are listed in columns 3, 5 and 6 of Table I, and the fully corrected γ ray intensities, expressed relative to that of the 829-keV peak, are given in Table IV where they are also compared with results from previous measurements.

Of the five previous measurements listed in Table I, the first four [20–23] report measurements of the β-delayed γ rays from the decay of ^{26}Si. The fifth is a ^{25}Mg (p,γ) ^{26}Al measurement [24], which yielded precise information on the γ-ray branching from the 1851-, 2072- and 2740-keV levels in ^{26}Al. Where they overlap, the agreement among all previous results is generally good, as is the agreement with our new results, which appear in the second to last column. Consequently, where actual values are quoted for a particular transition, we take weighted averages as our "adopted" values, with uncertainties multiplied by the square-root of the normalized chi-squared if necessary. Where only upper limits exist for a transition, we adopt the lowest.

IV. RESULTS

A. Gamow-Teller branching ratios

In Secs. III C, III D, and III E, we have assembled all the elements needed to evaluate the right-hand side of Eq. (1). We express the result as follows:

$$R'_{1058} = 0.2118(11), \tag{2}$$

where we have placed a prime on R to acknowledge that it refers specifically to the probability for producing a 829-keV γ ray following positron emission from ^{26}Si. To determine the total branching ratio to the 1058-keV level, we must take account of other γ transitions that could feed or deexcite the state, and of the electron-capture contribution to the β transition.

It can be seen from Fig. 9 that there are four potential γ-ray transitions, at 793, 1014, 1682 and 2666 keV, that could populate the 1058-keV level and one at 641 keV that could additionally depopulate it. We have established stringent upper limits on all five, which appear in Table IV. These do not affect the central value of R'_{1058}, and they have an imperceptible impact on its uncertainty.

To account for missing electron-capture decays, we must recognize first that both the numerator and denominator in Eq. 1 are affected. This means that our

TABLE V. Measured β-branching ratios to all the states in ^{26}Al populated by the β decay of ^{26}Si.

E_{x_i} [a]	$E_{\beta max}$	(β^+ + ec) branching		
(keV)	(keV)	Relative	Absolute	log ft
228.3	3818.8		0.7569(14)	3.4845(8)
1057.7	2989.4	$1.0000(^{+7}_{-8})$	0.2119(11)	3.558(2)
1850.6	2196.5	0.1310(20)	0.0278(4)	3.848(8)
2071.6	1975.5	$0.0134(^{+18}_{-8})$	$0.0028(^{+4}_{-2})$	$4.64(^{+4}_{-7})$
2740.0	1307.1	$0.0029(^{+11}_{-1})$	$0.0006(^{+2}_{-0})$	$4.55(^{+0}_{-11})$
3723.8	323.3	$0.0000(^{+2}_{-0})$	$0.00000(^{+3}_{-0})$	>5.8

[a] Values taken from Ref. [10]

result for R'_{1058} must be multiplied by $(1+\xi_{1058})/(1+\xi)$, where ξ_{1058} is the electron-capture-to-positron ratio for the β transition populating the 1058-keV state and ξ is the ratio for the total decay of ^{26}Si. Using the $ec/\beta^+(\equiv \xi)$ values listed in Table I, we determine that $(1+\xi_{1058})/(1+\xi) = 1.00132/1.00088 = 1.00044$. Applying this correction factor to R'_{1058}, we determine the final branching ratio for the $(\beta + ec)$ transition to the 1058-keV state in ^{26}Al to be

$$R_{1058} = 0.2119(11). \quad (3)$$

This result appears in the second row, fourth column of Table V.

We calculate the branching ratios for the Gamow-Teller transitions to other levels in ^{26}Al the same way. For each level, the $(\beta + ec)$ feeding is determined from the total γ-ray intensity that depopulates the level, minus the total γ-ray intensity observed to populate it. We use the normalized intensities listed in the last column of Table IV, taking the placement of each γ-ray transition from the level scheme in Fig. 9. The results, still normalized to the 829-keV γ-ray intensity, are listed in column 3 of Table V. Those results multiplied by R_{1058} yield the final branching ratios, which appear in the next column. Since the electron-capture contributions are accounted for in both Eq. (3) and Table IV, no further adjustment was required to obtain the branching ratios.

We determined the log ft values for the Gamow-Teller transitions using the log ft calculator available at the National Nuclear Data Center website [25]. In addition to a branching ratio, the input data for each transition included the corresponding decay energy, $E_{\beta max}$, as listed in Table V, and the half-life of ^{26}Si taken from the most recent survey of world data for superallowed emitters [1], 2245.3(7) ms. The resulting log ft values appear in the last column of the table. All values, including the >5.8 lower limit, are well within expectations for allowed $0^+ \to 1^+$ transitions [26].

It is apparent in Fig. 9 that the 3^+ state at 417 keV in ^{26}Al is also populated and depopulated by γ rays, albeit weak ones. From the information in Table IV, we determine the total γ-ray feeding to be $0.0023(^{+7}_{-1})$ and the total decay to be 0.0027(8), both expressed relative to the 829-keV γ-ray intensity. These values are consistent with there being no side-feeding from β decay, a conclusion expected for a well established 3^+ state [10], which could only be fed by a second-forbidden-unique β transition with a log ft value of 14 or more [26]. Obviously, we have made no provision for this transition in our quoted branching ratios.

B. Branching ratio for the superallowed transition

The states at 1058, 1851, 2072, 2740 and 3724 keV are all fed by Gamow-Teller transitions with branching ratios (and one upper limit) listed in Table V. Their total, with uncertainties carefully taken account of, is 0.2431(14). Shell-model calculations to be presented in Sec. V A rule out the possibility that any β-decay strength could be dissipated into numerous more highly excited states: *i.e.* the pandemonium effect [27, 28] can be excluded.

Thus, the branching ratio for the superallowed $0^+ \to 0^+$ transition to the 228-keV analog state becomes 0.7569(14), a result obtained by subtraction of the total Gamow-Teller branching ratio from unity. By this simple subtraction, we have converted the relative precision obtained in our measurement, which is 0.58% (=0.0014/0.2431), to a relative precision of 0.18% (=0.0014/0.7569) for the superallowed branching ratio, the quantity of interest. For the superallowed transition, where the greatest precision is required, we used the full calculation for the statistical rate function, f, as described in Ref. [1]. The branching ratio and the resulting log ft value appear in the top line of columns 4 and 5 in Table V.

TABLE VI. Uncertainty budget for ^{26}Si branching ratios.

Source	Uncertainty (%)	
	Σ GT branches	$0^+ \to 0^+$ branch
Counting statistics:		
γ_{829} and β singles	0.44	0.14
$\Sigma\gamma/\gamma_{829}$	0.17	0.05
Coincidence summing with 511-keV γ's	0.14	0.04
Systematics:		
HPGe detector efficiency	0.20	0.06
Dead time	0.14	0.05
Bremsstrahlung coincidence summing	0.10	0.03
Relative β-detector efficiencies	0.10	0.03
^{26}Si component of β singles	0.07	0.02
Random preemption of real coincidences	0.02	0.01
Total uncertainty	0.58	0.18

C. Uncertainty budget

The uncertainty budget for our ^{26}Si branching-ratio measurement is given in Table VI. For each contribution we give two relative uncertainties, both in percent. The first is expressed relative to the Gamow-Teller-branch total and thus characterizes the measurement itself. The second is expressed relative to the superallowed branching ratio and illustrates the contribution's impact on the quantity of principal interest.

By far the largest contribution to the total uncertainty comes from the counting statistics for the 829-keV γ ray and the β singles. The decays of ^{26}Si and ^{26m}Al, which of necessity we recorded together, are dominated by positrons and positron-annihilation radiation. In fact, the 829-keV γ-ray peak in our HPGe detector represents only about 1% of the total counts in the spectrum. In order not to degrade the quality of our data, we had to

TABLE VII. Experimental and theoretical excitation energies and β-decay branching ratios, R, to the daughter 1^+ states in ^{26}Al. The theoretical values were obtained from *sd* shell-model calculations with effective interactions USD, USD-A and USD-B.

State	Expt.		USD		USD-A		USD-B	
	E_x (keV)	R(%)	E_x (keV)	R(%)	E_x (keV)	R(%)	E_x (keV)	R(%)
$1^+_1, T=0$	1058	21.9	955	21.7	793	18.8	1022	19.9
$1^+_2, T=0$	1851	2.73	1994	3.07	1900	3.68	1890	3.15
$1^+_3, T=0$	2071	0.290	2260	0.261	2082	0.064	2184	0.026
$1^+_4, T=0$	2740	0.062	3118	0.050	2744	0.134	2828	0.110
$1^+_5, T=0$	3724	<0.0002	3851	0.000006	3767	0.00045	3669	0.00029
$1^+_6, T=0$	5010	—	5194	—	5255	—	5008	0.00000

limit the overall counting rate, so this naturally limited the number of 829-keV events we could collect during a seven day measurement. In fact, all three items listed under "counting statistics" were similarly dependent on our imposed counting-rate limitations.

The contributions listed under "systematics" in the table all stem from effects that are inherent to our basic equipment and techniques. Their total contribution to the overall uncertainty is about two-thirds that of the counting statistics.

V. DISCUSSION

A. Gamow-Teller branches

The shell model has proven to be remarkably successful in describing the energy levels and decays of *sd*-shell nuclei like ^{26}Si and ^{26}Al [29–31]. How successful it is for the β-decay branching ratios we have measured can be seen from Table VII. There we compare our results with those of *sd*-shell calculations for 1^+ states in ^{26}Al based on the USD effective interaction of Wildenthal [29] and on two more-recent updates, USD-A and USD-B, of Brown and Richter [30]. For all three, we use a quenched value for the axial-vector coupling constant, $g_{A,eff} = 1$, which Brown and Wildenthal [31] demonstrated to be appropriate for use in calculations truncated to just *sd*-shell configurations.

In Table VII we show results for the six lowest energy 1^+ states in ^{26}Al. Since the Q_{EC} value for ^{26}Si β decay to the ground state is 5069 keV, we have ignored states lying well above that energy since they are inaccessible to β decay. Overall, the agreement between theory and experiment is very good, with the USD calculation doing a particularly good job of reproducing the experimental branching ratios.

It is critically important in precise β decay studies to be able to rule out – or, if necessary, correct for – the possibility of there being numerous individual branches to highly excited states, which are too weak to detect individually but collectively are intense enough to influence the results [27, 28]. All three models in Table VII predict only one possible state between the 3724-keV level and the energy region around the upper limit of the Q_{EC}-value window; and this state, if accessible at all, would be negligibly fed by β decay. We can confirm then that the set of branching ratios listed in Table V is complete.

B. Superallowed decay branch and mirror comparison

Although there have been several previous measurements of the relative intensities of β-delayed γ rays from the decay of ^{26}Si (see Table IV), only two were able to determine the absolute branching ratio for the superallowed β-decay branch: one from 1975, which quoted 0.749(9) [21], and one from 2008, which found 0.757(23) [23]. Our result, 0.7569(14), agrees with both but has reduced the uncertainty by a factor of 6 over the best of the two.

Since the Q_{EC} value for the superallowed decay branch has not been improved since the last survey of world data [1], we adopt the f value of 1028.03(12) given in Table IX of that reference. Similarly we adopt the half-life, 2245.3(7) ms, from Table III of the same reference, since it has not changed either. In combination with our new branching-ratio result, these values yield

$$ft = 3051.5(57)s \tag{4}$$

for the superallowed branch.

This ft value is still subject to radiative and isospin-symmetry-breaking corrections, so it is conventional to define a corrected $\mathcal{F}t$, which can ultimately be used to extract V_{ud}. It is defined by

$$\mathcal{F}t = ft(1+\delta'_R)(1+\delta_{NS}-\delta_C), \tag{5}$$

where δ_C is the isospin-symmetry-breaking correction and the terms δ'_R and δ_{NS} comprise the transition-dependent part of the radiative correction, the former being a function only of the positron's energy and the atomic number of the daughter nucleus, while the latter, like δ_C, depends in its evaluation on the details of nuclear structure. Taking the values for these three small correction terms from Table IX of Ref. [1], we obtain

$$\mathcal{F}t = 3075.3(59)s. \tag{6}$$

The relative uncertainty of this result is 0.19%, which is competitive with the 14 previously best-known superallowed emitters and is consistent with their average of $\overline{\mathcal{F}t} = 3072.27(62)$ s. This is the first time that the ^{26}Si superallowed transition has become eligible to join the ranks of transitions known precisely enough to contribute to the evaluation of V_{ud}.

Our new branching-ratio result for ^{26}Si has a more important consequence though. Not only does it lead to the first precise ft value for the ^{26}Si superallowed branch, but it also completes a mirror pair of precisely characterized superallowed transitions: $^{26}\text{Si} \rightarrow {}^{26m}\text{Al}$ and $^{26m}\text{Al} \rightarrow {}^{26}\text{Mg}$. This is only the second such precisely known pair, the first being the decays of ^{38}Ca and ^{38m}K. As first proposed for the $A = 38$ pair [4], the ratio of ft values for the two mirror transitions can lead to a sensitive test of the calculated charge-dependent corrections that appear in Eq. 5.

If one accepts the constancy of $\mathcal{F}t$, the ratio of ft values for a pair of mirror superallowed transitions can be written as,

$$\frac{ft^a}{ft^b} = 1 + (\delta_R^{'b} - \delta_R^{'a}) + (\delta_{NS}^b - \delta_{NS}^a) - (\delta_C^b - \delta_C^a) \quad (7)$$

where superscript "a" denotes the decay of the $T_Z = $-1 parent and "$b$" the decay of the $T_Z = 0$ parent. As explained in Refs. [1, 4], the advantage offered by Eq. (7) is that the theoretical uncertainty on a difference term such as $(\delta_C^b - \delta_C^a)$ is significantly less than the uncertainties on δ_C^b and δ_C^a individually. Different models for isospin symmetry breaking produce non-overlapping predictions for the ft ratio, which can then be compared with the experimental ratio.

In particular, two models have been used previously to calculate δ_C, with the numerical difference between the results determining the theoretical uncertainty attached to δ_C [32]. One model employed Woods-Saxon radial wave functions and the other, Hartree-Fock ones. The predicted ft^a/ft^b ratios for both models as applied to four selected mirror pairs appears in Table I in Ref. [4]. We plot them as shaded bands in Fig. 10, where it can be seen that one model's predictions are cleanly separated from the other's.

In evaluating the experimental ft^a/ft^b ratio for the mass-26 pair, we take our measured ft value from Eq. (4) as ft^a and the ^{26m}Al ft value from the most recent survey [1] as ft^b. The result for ft^a/ft^b is 1.0046(19). This value agrees with 1.0039(3), the ratio obtained if Woods-Saxon radial wave functions are used to calculate δ_C, and disagrees with the 1.0019(3) ratio obtained if Hartree-Fock functions are used. The measured mass-26 ratio is also plotted in Fig. 10 along with the previous mass-38 result [5], where they are visually compared with the two sets of calculations. Both measurements are consistent in favoring the Woods-Saxon calculations over the Hartree-Fock ones.

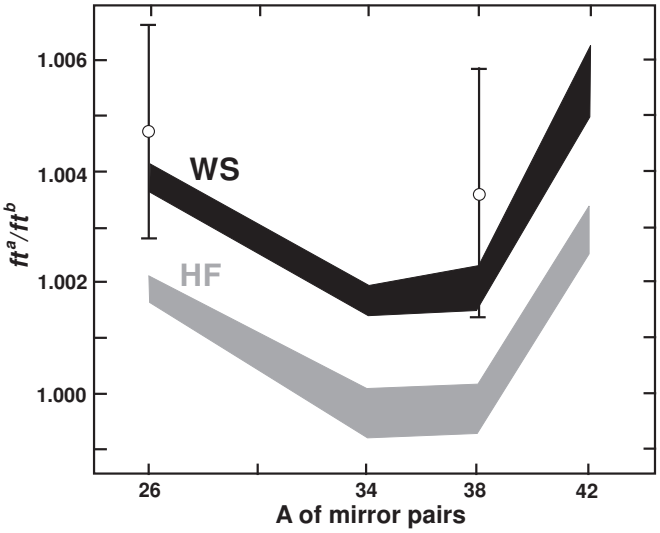

FIG. 10. Mirror pair ft^a/ft^b values for $A = 26$, 34, 38 and 42. The black and grey bands connect calculated results that utilize Woods-Saxon (WS) and Hartree-Fock (HF) radial wave functions, respectively, to evaluate δ_C. The open circles with error bars are the measured results for the mass-26 pair, from this measurement, and the mass-38 pair from Ref. [4, 5].

VI. CONCLUSIONS

We have determined the branching ratio for the superallowed $0^+ \rightarrow 0^+$ β-decay transition from ^{26}Si to be 0.7569(14), a result with 0.18% relative precision. It is the first measurement of this quantity to have subpercent precision. Since both the Q_{EC} value and half-life for the transition are already well known, the derived $\mathcal{F}t$ value of 3074.5(59) s is, for the first time, precise enough to be placed among the precisely measured $\mathcal{F}t$ values used to derive V_{ud} [1]. This is the first addition to that select group since ^{38}Ca was added five years ago [4].

Of particular significance, our branching-ratio result also provides the last link needed to complete the ft-value information for a second pair of superallowed mirror transitions, $^{26}\text{Si} \rightarrow {}^{26m}\text{Al}$ and $^{26m}\text{Al} \rightarrow {}^{26}\text{Mg}$. The resultant ft^a/ft^b ratio for the mass-26 mirror pair favors the use of Woods-Saxon radial wave functions over Hartree-Fock ones in the calculation of δ_C, the isospin-symmetry-breaking correction needed for the extraction of V_{ud}. This reinforces the same provisional conclusion reached for the equivalent mass-38 ratio, measured previously [4], and supports the decision made in the last survey of world data [1] no longer to use the Hartree-Fock calculations as a measure of systematic theoretical uncertainty in δ_C.

Finally, we have found that our measured Gamow-Teller β-decay branching ratios to 1^+ states in ^{26}Al are in excellent agreement with shell-model calculations. Since those same *sd*-shell calculations played a role in determining δ_C and δ_{NS} in the region [1, 33], this further

increases confidence in those determinations.

ACKNOWLEDGMENTS

This work was supported by the U.S. Department of Energy under Grant No. DE-FG03-93ER40773 and by the Welch Foundation under Grant No. A-1397.

[1] J. C. Hardy and I. S. Towner, Phys. Rev. C **91**, 025501 (2015).
[2] J. C. Hardy and I. S. Towner, *Proceedings of the 13th International Conference on the Intersections of Particle and Nuclear Physics, (CIPANP2018)*, eds: B. Casey and W. Haxton, eConf C18-05-29, 25 (2018), arXiv: 1807.01146.
[3] C.-Y. Seng, M. Gorchtein, H. H. Patel and M. J. Ramsey-Musolf, Phys. Rev. Lett. **121**, 241804 (2018).
[4] H. I. Park, J. C. Hardy, V. E. Iacob, M. Bencomo, L. Chen, V. Horvat, N. Nica, B. T. Roeder, E. Simmons, R. E. Tribble, and I. S. Towner, Phys. Rev. Lett. **112**, 102502 (2014).
[5] H. I. Park, J. C. Hardy, V. E. Iacob, M. Bencomo, L. Chen, V. Horvat, N. Nica, B. T. Roeder, E. McCleskey, R. E. Tribble, and I. S. Towner, Phys. Rev. C **92**, 015502 (2015).
[6] R. E. Tribble, A. Azahari, C. A. Gagliardi, J. C. Hardy, A. Mukhamedzhanov, X. Tang, L. Trache, and S. J. Yennello, Nucl. Phys. A **701** (2002).
[7] Acuity AR700-4 Laser Displacement Sensor, http://www.acuitylaser.com.
[8] Arduino, http://www.arduino.cc.
[9] J. F. Ziegler, http://www.srim.org.
[10] M. S. Basunia and A. M. Hurst, Nuclear Data Sheets **134**, 1 (2016).
[11] R. G. Helmer, J. C. Hardy, V. E. Iacob, M. Sanchez-Vega, R. G. Nielson, and J. Nelson, Nucl. Instrum. Methods in Phys. Res., Sect. A **511**, 360 (2003).
[12] E. Schönfeld, H. Janssen, R. Klein, J. C. Hardy, V. Iacob, M. Sanchez-Vega, H. C. Griffin and M. A. Ludington, Appl. Radiat. Isot. **56**, 215 (2002).
[13] J. A. Halbleib, R. P. Kemsek, T. A. Mehlhorn, S. M. S. G. D. Valdez, and M. J. Berger, Report SAND91-16734, Sandia National Labs, 1992.
[14] R. G. Helmer, N. Nica, J. C. Hardy, and V. E. Iacob, Int. J. Appl. Radiat. Isot. **60**, 173 (2004).
[15] S. Agostinelli *et al.*, Nucl. Instrum. Methods in Phys. Res. A **506**, 250 (2003).
[16] V. V. Golovko, V. E. Iacob, and J. C. Hardy, Nucl. Instrum. Methods in Phys. Res. A **594**, 266 (2008).
[17] I. Kawrakow, Med. Phys. **27**, 485 (2000); I. Kawrakow and D. W. O. Rogers, NRCC Report PIRS-701, NRC, Ottawa (2003); http://www.irs.inms.nrc.ca/EGSnrc/EGSnrc.html.
[18] D. C. Radford, Nucl. Instrum. Methods in Phys. Res. A **361**, 297 (1995).
[19] E. A. McCutchan, Nucl. Data Sheets **113**, 1735 (2012).
[20] C. E. Moss, C. Detraz, and C. S. Zaidins, Nucl. Phys. A **174**, 408 (1971).
[21] J. C. Hardy, H. Scheming, J. S. Geiger, and R. L. Graham, Nucl. Phys. A **246**, 61 (1975).
[22] H. S. Wilson, R. W. Kavanagh, and F. M. Mann, Phys. Rev. C **22**, 1696 (1980).
[23] I. Matea, J. Souin, J. Aysto, B. Blank, P. Delahaye, V.-V. Elomaa, T. Eronen, J. Giovinazzo, U. Hager, J. Hakala, J. Huikari, A. Jokinen, A. Kankainen, I. D. Moore, J.-L. Pedroza, S. Rahaman, J. Rissanen, J. Ronkainen, A. Saastamoinen, T. Sonoda and C. Weber, Eur. Phys. J. A **37**, 151 (2008); erratum **38**, 247 (2008).
[24] P. M. Endt, P. De Wit, and C. Alderliesten, Nucl. Phys. A **476**, 333 (1988).
[25] National Nuclear Data Center, www.nndc.bnl.org.
[26] B. Singh, J. L. Rodriguez, S. S. M. Wong and J. K, Tuli, Nuclear Data Sheets **84**, 487 (1998).
[27] J. C. Hardy, L. C. Carraz, B. Jonson and P. G. Hansen, Phys. Lett. B **72**, 307 (1977).
[28] J. C. Hardy and I. S. Towner, Phys. Rev. Lett. **88**, 252501 (2002).
[29] B. H. Wildenthal, Prog. Part. Nucl. Phys. **11**, 5 (1984).
[30] B. A. Brown and W. A. Richter, Phys. Rev. C **74**, 034315 (2006).
[31] B. A. Brown and B. H. Wildenthal, At. Data and Nucl. Data Tables **33**, 347 (1985).
[32] J. C. Hardy and I. S. Towner, Phys. Rev. C **79**, 055502 (2009).
[33] I. S. Towner and J. C. Hardy, Phys. Rev. C **77**, 025501 (2008).